Biocybernetics and Biomedical Engineering 44 (2024) 814–823

Contents lists available at ScienceDirect

Biocybernetics and Biomedical Engineering

journal homepage: www.elsevier.com/locate/bbe

Research Paper

Probabilistic and explainable modeling of Phase–Phase Cross-Frequency Coupling patterns in EEG. Application to dyslexia diagnosis

Diego Castillo-Barnes [a,b,*], Nicolás J. Gallego-Molina [a], Marco A. Formoso [a], Andrés Ortiz [a], Patrícia Figueiredo [b], Juan L. Luque [c]

[a] Department of Communications Engineering, University of Malaga, Blvd. Louis Pasteur 35, Malaga, 29010, Malaga, Spain
[b] Institute for Systems and Robotics (Lisboa/LARSyS) and Department of Bioengineering, Instituto Superior Técnico, Universidade de Lisboa, Av. Rovisco Pais 1, Lisbon, 1049-001, Lisbon, Portugal
[c] Department of Developmental and Educational Psychology, University of Malaga, Dr. Ortiz Ramos 12, Malaga, 29010, Malaga, Spain

ARTICLE INFO

Keywords:
Mixture models
Cross-Frequency Coupling
EEG
Signal processing
Explainable machine learning
Dyslexia

ABSTRACT

This work explores the intricate neural dynamics associated with dyslexia through the lens of Cross-Frequency Coupling (CFC) analysis applied to electroencephalography (EEG) signals evaluated from 48 seven-year-old Spanish readers from the LEEDUCA research platform. The analysis focuses on CFS (Cross-Frequency phase Synchronization) maps, capturing the interaction between different frequency bands during low-level auditory processing stimuli. Then, making use of Gaussian Mixture Models (GMMs), CFS activations are quantified and classified, offering a compressed representation of EEG activation maps. The study unveils promising results specially at the Theta-Gamma coupling (Area Under the Curve = 0.821), demonstrating the method's sensitivity to dyslexia-related neural patterns and highlighting potential applications in the early identification of dyslexic individuals.

1. Introduction

According to the World Health Organization (WHO), dyslexia is a neurodevelopmental disorder that affects reading and language skills. Early identification is crucial for providing tailored instruction and accommodations, significantly improving reading abilities and overall academic success for children with dyslexia. Intervention at these stages also boosts self-esteem and confidence, preventing potential academic struggles.

Current methods for identifying children with dyslexia typically involve a combination of standardized reading and language assessments, along with observations and teacher reports [1]. These assessments evaluate a child's reading accuracy, fluency, and comprehension. If a child consistently lags behind their peers in reading skills despite adequate instruction, it may raise concerns about dyslexia. However, the specific criteria and timing for identification can vary, and additional neuropsychological or medical evaluations may be needed for a formal diagnosis [2].

One of the major limitations of these approaches is the reliance on standardized reading tests, which may not capture the full spectrum of dyslexia's characteristics. Dyslexia is not solely a reading disorder; rather, it is a complex and heterogeneous condition involving underlying neurocognitive and neural processing differences [3–5]. To address these complexities, we can utilize tools such as Cross-Frequency Coupling (CFC) measures[1] from electroencephalography (EEG) signals, which preserve spatial and temporal information in neural communication across frequency bands. This approach is effective in discerning neural and cognitive differences between healthy and dyslexic children, revealing dyslexia-specific neural networks and cognitive processes involved in dyslexic difficulties [6–10].

In the last years, the integration of artificial intelligence techniques for analyzing EEG bands, especially CFC values, has yielded significant insights into dyslexia's biological underpinnings. Noteworthy contributions in this field provide valuable context for our work. In [11], Principal Component Analysis (PCA) was employed to reveal dyslexia patterns in 7-year-old children, offering a temporal evolution of PAC-based connectivity and demonstrating discriminative capabilities, notably in the Beta-Gamma bands. [12] delves into changes and patterns of CFC in developmental dyslexia using a Holo-Hilbert Spectral Analysis (HHSA) approach, providing a complementary method to unveil intricate dynamics. In [13], phase synchronization in brain networks during auditory processing was explored, revealing differences between dyslexic individuals and controls. This auditory focus

* Corresponding author at: Department of Communications Engineering, University of Malaga, Blvd. Louis Pasteur 35, Malaga, 29010, Malaga, Spain.
E-mail address: diegoc@uma.es (D. Castillo-Barnes).

[1] This term encompasses both Phase-Phase coupling (also known as Cross-Frequency phase Synchronization, CFS) and Phase-Amplitude Coupling (PAC).

https://doi.org/10.1016/j.bbe.2024.09.003
Received 6 April 2024; Received in revised form 5 September 2024; Accepted 12 September 2024
Available online 21 October 2024

offers valuable insights into the specific neural processes underlying dyslexia in response to auditory stimuli. [14] conducted a complex network analysis of brain coupling during auditory stimuli presentation, utilizing graph theory metrics to enhance differentiation with Support-Vector-Machine (SVM) classifiers. This network-centric approach adds a layer of complexity to the analysis which improves our understanding of dyslexia-related brain connectivity. Lastly, [15] investigates neural mechanisms of speech processing in infants, emphasizing low-frequency cortical tracking and PAC. Using a multivariate temporal response function (mTRF) method, the study established significant delta and theta tracking of speech stimuli. Additionally, PAC in some bands indicated the presence and maturation of low-frequency cortical speech tracking in infants which suggests a role for PAC in the development of speech processing.

Although these types of analyses are very promising, the inherent noise in EEG signals as well as the heterogeneous nature of dyslexia may hinder the identification of subtle but highly relevant patterns. In this context, the proposal of new markers based on CFC values should consider two aspects: (1) they should avoid the loss of interpretability, as seen with approaches that use PCA or PLS [11]; and (2) they should improve the results obtained by directly analyzing CFC measures in the bands of interest, regardless of the classifier used. Our histogram transformation method addresses these concerns by enhancing the discernment between controls and dyslexics. Unlike the Pixels-As-Features approach or PCA, our method uses significantly fewer input features, yet achieves comparable or better results. This is true irrespective of the classifier employed. Additionally, our method could potentially identify which brain areas are most related to dyslexia and those that result from indirect coupling between brain signals (confoundings) [16–18]. This enhancement in CFS maps offers a robust tool for understanding the neural underpinnings of dyslexia.

Based on these assumptions, for this study, we first perform a histogram transformation on the CFS maps to enhance the differences between controls and dyslexic children. This transformation replaces the activations of each pixel in the CFS intensity maps with the height of their corresponding histogram bins, accentuating the edges of regions in the CFS maps. This step aids in clustering and classification tasks by making the distinctions between different regions more pronounced. Following this, we apply a 3D Gaussian Mixture Model (GMM) to quantify the transformed CFS activations at different coupling levels (Theta-Gamma, Alpha-Beta, and Beta-Gamma bands). The GMM-based quantization helps reduce the dimensionality of the input data, particularly when dealing with high-dimensional EEG activation maps. By compressing the representation of the input activation maps, our approach captures essential features while discarding less relevant details. This not only makes the subsequent classification task more computationally efficient but also less prone to overfitting [19].

Our method involves classifying the CFS maps using no more features than the number of components in the GMM model, typically no more than 20 features. This is a significant reduction compared to classifying the original 32×32 pixel images, or a reduced dimensional space with PCA but still larger than 20. This dimensional reduction prevents overfitting and enhances robustness to variations in the input data.

We have evaluated this approach using synthetic data and real EEG data, demonstrating its effectiveness in enhancing intensity differences and improving classification outcomes. Our method consistently outperforms both the traditional Pixels-As-Features (PAF) and PAF combined with PCA methods in most cases, highlighting its robustness and efficiency in differentiating between dyslexic and control groups.

After exploring the contextual background and limitations of dyslexia assessment techniques in this section, the rest of this contribution is structured as follows. First, in Section 2, we describe the dataset we have used to evaluate our proposal and introduce the application of the histogram transformation and the use of Gaussian Mixture Models to evaluate CFC values. Then, in Section 3, we present the empirical findings obtained. These results are interpreted in Section 4 and compared to the current literature, addressing limitations and suggesting future directions. Finally, in Section 5 we synthesize our contribution, emphasizing the implications for advancing dyslexia research and neuroscientific evaluation methodologies.

2. Materials & methods

2.1. Database

The dataset used in this study was sourced from the LEEDUCA research group at the University of Malaga (Spain) [20], originating from a longitudinal study involving over 1400 children aged 4 to 8 years. Participants were selected through quarterly assessments employing a comprehensive battery of cognitive and linguistic tasks. From this cohort, 15 children with a confirmed diagnosis of dyslexia and 33 with no discernible impairment were chosen, ensuring matching age and socio-economic indices on a 1–10 scale. During EEG sessions, participants were exposed to amplitude-modulated white noise at rates of 4.8 Hz, 16 Hz, and 40 Hz, representing core speech units in the Spanish language. Each 15-minute session included sequential presentation of stimuli in ascending and descending order (4.8 - 16 - 40 - 40 - 16 - 4.8 Hz). EEG signals were acquired using Brainvision actiCHamp Plus with actiCAP electrodes (Brain Products GmbH, Germany) in a 32-channel 10–20 configuration optimized for auditory processing, sampled at 500 Hz. Post-acquisition processing involved the removal of eye blink artifacts using Independent Component Analysis (ICA),[2] channel-wise normalization to zero mean and unit variance, referencing to the Cz electrode, and baseline correction. The study adhered to ethical guidelines, with written consent from guardians, approval from the Medical Ethical Committee of Málaga University (Ref. CEUMA 16−2020−H), and compliance with the World Medical Association Declaration of Helsinki. Support for the research was granted by the Education Office of the regional government of Andalusia (Spain), facilitating its execution in various public schools.

2.2. Computing CSF maps from EEG signals

The CFC measures in EEG signals help us to measure how different frequency oscillations in the brain coordinate and interact. In the case of the CFS, we specifically refer to how the phase of one frequency band influences on the phase of another frequency band [25]. This phenomenon is crucial for understanding how neural networks communicate and synchronize, playing a vital role in various cognitive processes such as memory, attention, and perception [26].

In this work we focus on the distribution of phase angle differences between frequency bands for assessing CFS in neuronal oscillations as introduced in [27–29]. To measure the $n : m$ phase-locking we have computed the length of the mean vector arisen from a distribution of unitary vectors whose angle is the instantaneous phase difference between two frequency bands in the same electrode. Thus, the potential couplings between two frequency bands are those described in (1) where N is the number of time points, and $\phi_A(t)$ and $\phi_B(t)$ are the phase angles for the frequency bands A and B respectively. In our analysis, we fixed n at 1 and iterated m from 1 to 10, exploring a range of phase-locking scenarios by varying the phase acceleration of the lower frequency band. This approach helped us to identify the optimal m that provides the highest statistically significant coupling.

$$\mathrm{CFS}_{A,B} = \left| \frac{1}{N} \sum_{t=1}^{N} e^{i(n\cdot\phi_A(t) - m\cdot\phi_B(t))} \right| \tag{1}$$

[2] While effective in removing artifacts, ICA may slightly affect EEG signal phase [21]. Recent studies support its use for phase connectivity analysis [22], in the context of ocular artifact removal since the mixing process is approximately linear [23,24].

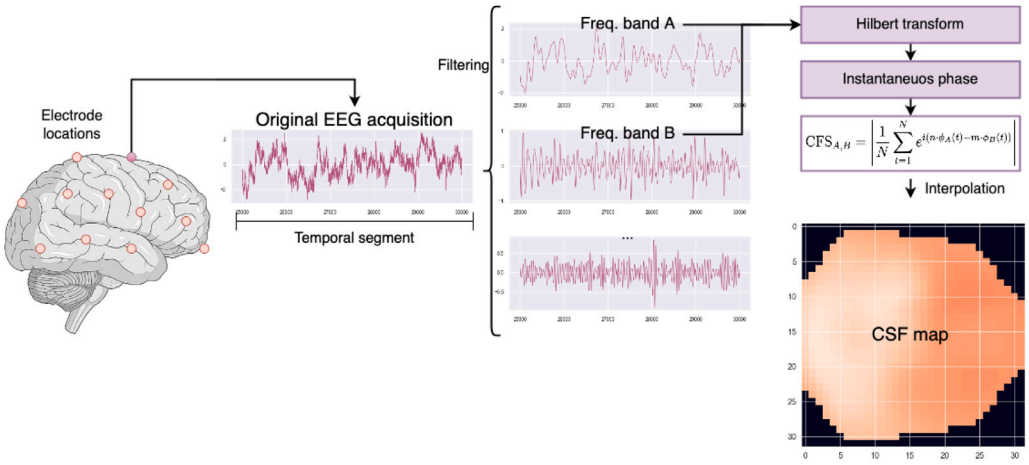

Fig. 1. Evaluation of CFS values from EEG signals. In each electrode we compute CFS values for each temporal segment and between the selected frequency bands. Having done the projection of the electrode locations onto a 2D space, we can represent these CFS values as a image that preservers the spatial information.

In any case, and similar to other phase-based coupling analyses, we also operate under the assumption that when functional coupling exists between brain rhythms, the timing of their oscillatory processes becomes synchronized.

To get to the calculation of CFS values in (1), we first have to filter our input EEG signals to extract the bands of interest. In this case, we will focus on Delta (0.5–4 Hz), Theta (4–8 Hz), Alpha (8–12 Hz), Beta (12–30 Hz) and Gamma (30–80 Hz) bands. Following the recommendations given in [30], we have made use of two-ways (forward–backward) Finite Input Response (FIR) filters to avoid phase shift or distortion, ensuring that phase relationships within the EEG frequency bands are maintained. If we refer to $x(t)$ as the given EEG band-filtered signal of interest, we can determine its instantaneous phase, $\phi(t)$, by means of the Hilbert Transform[3] in (2), and the computation of its argument in (3) [31].

$$z(t) = x(t) + j \cdot H[x(t)] \qquad \text{where} \qquad H[x(t)] = \frac{1}{\pi} \int_{-\infty}^{+\infty} \frac{x(t)}{t-\tau} d\tau \tag{2}$$

$$\phi(t) = \angle z(t) = \text{atan2}\Big(\Im(z(t)), \Re(z(t))\Big) \tag{3}$$

Though the representation of the CFS values in (1) between two frequency bands can be estimated for the whole time interval, it is more interesting to segment each $\phi(t)$ signal into smaller time sequences (e.g. each of 5 s) and represent their temporal evolution. However, since the spatial location of the EEG electrodes belong to a 3-D space, the visualization of our final results will also require the projection of each electrode to a reference space in 2-D. For that, if we assume that the EEG electrodes locations can be approximated by a sphere, then we can apply a projection such as the Azimuthal Equidistant Projection method employed in [32]. Thus, using the measures from the 31 electrodes for a pair of EEG frequency bands and interpolating their results by means of (for example) the Clough–Tocher interpolation scheme described in [33], we can fill the space between the cloud of CFS values and get a map showing the spatial phase-phase coupling distribution between frequency bands. A diagram showing this procedure has been depicted in Fig. 1.

[3] Taken in the sense of the Cauchy principal value, which accounts for singularities in the integrand.

2.2.1. CSF maps over time

The generation of CFS maps is performed iteratively for each time segment across input EEG sequences. While this procedure is applicable to any interaction between different frequency bands, our analysis will now specifically focus on evaluating Theta-Gamma, Alpha-Beta, and Beta-Gamma couplings, as they have been recognized as particularly promising for assessing differences in entrainment to speech [11,13, 34–36].

Until now, the temporal segments compose a sequence of images that represents the evolution of the phase synchronization alongside the spatial information of the EEG channel locations [37]. However, since the differences within these CFS layers might be subtle, we propose using a temporal averaging approach, by aggregating the sequence of images over time, to create a composite image that encapsulates the overarching development of phase synchronization across the EEG channel locations. This temporal averaging does not only facilitate a more comprehensive understanding of the cumulative effects but also aids in discerning variations that may be imperceptible in individual frames. On the other hand, this methodology has sense in or experimental setup since the auditory stimulus used is constant and does not require any user interaction.

2.3. Enhancing differences in CFS maps

When analyzing the CFS intensity maps (as shown in Fig. 2) and their associated histograms (Fig. 3), it becomes apparent that the histograms are relatively narrow (impulsive responses and asymmetric behavior) due to the low intensity differences present in the original images. This characteristic poses a challenge for classifiers as the distinctions between controls and dyslexics are subtle.

Based on this limitation, we propose a transformation of the CFS intensity maps where the activations of each pixel are replaced by the height associated with the bin of the histogram to which it belongs. This transformation effectively accentuates the edges of the regions in the CFS maps, aiding in clustering and classification tasks. Fig. 4 proves this enhancement visually, showing the impact of the transformation on the CFS maps in the Alpha-Beta coupling bands.

To validate the effectiveness of this approach across different signal types, including those lacking distinct isolated activations, we conducted experiments using synthetic PAC signals that emulate EEG sensor involvement. The synthetic signals were subject to background noise ($\sim \mathcal{N}(0, 0.5)$) and smoothing filters (Gaussian blur filtering using a 5×5 kernel), aiming to decrease the intensity variance across regions. As illustrated in Fig. 5, our proposed histogram transformation successfully enhances the intensity differences across regions

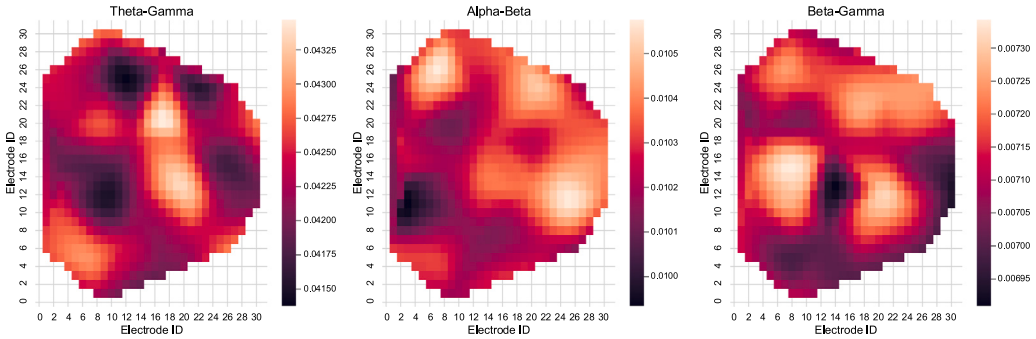

Fig. 2. CFS activations referred to different coupling bands for our EEG analysis. Results obtained when averaging the controls of the LEEDUCA platform dataset after applying the white noise auditory stimulus at 4.8 Hz.

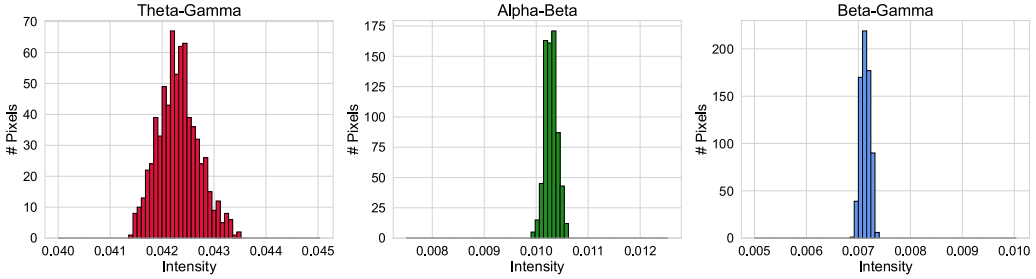

Fig. 3. Histograms illustrating the distribution of intensity values in the CFS maps for different coupling bands. Narrow histograms indicate limited contrast in the original intensity values, motivating the need for enhancement techniques.

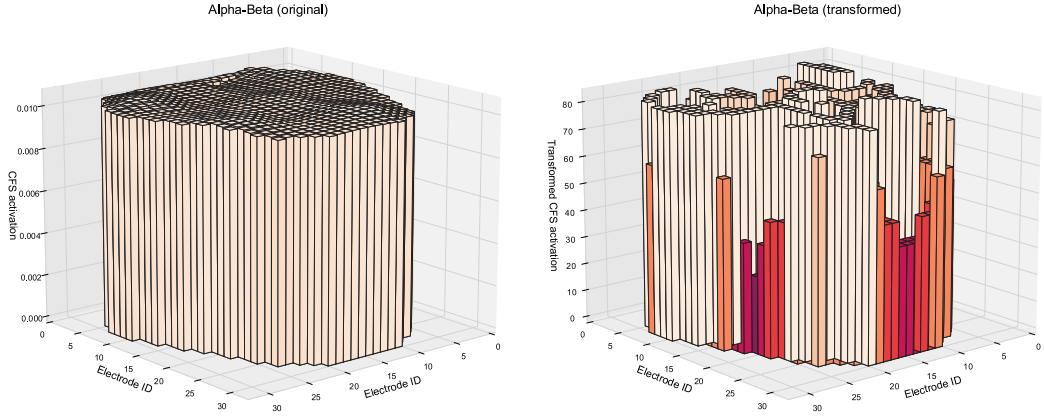

Fig. 4. Comparison of CFS map activations in the Alpha-Beta coupling bands before (left) and after (right) transformation using histogram-based enhancement. The transformation accentuates the edges of regions, improving contrast and aiding the identification of patterns to discern between controls and children with dyslexia.

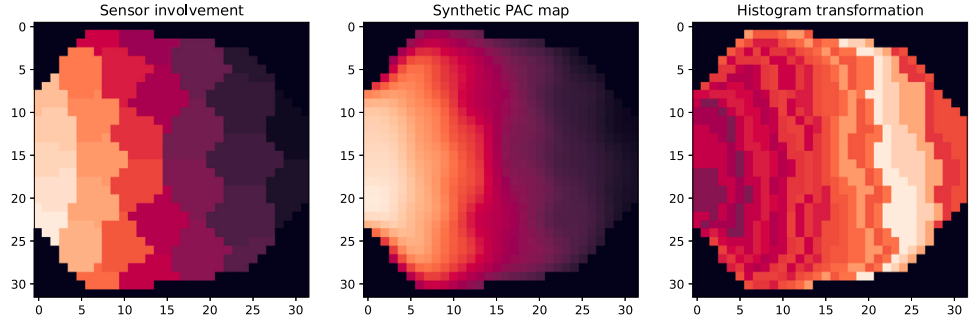

Fig. 5. 2D representation of synthetic activations before (left) and after (right) replacing its values by the heights of the bins associated to them.

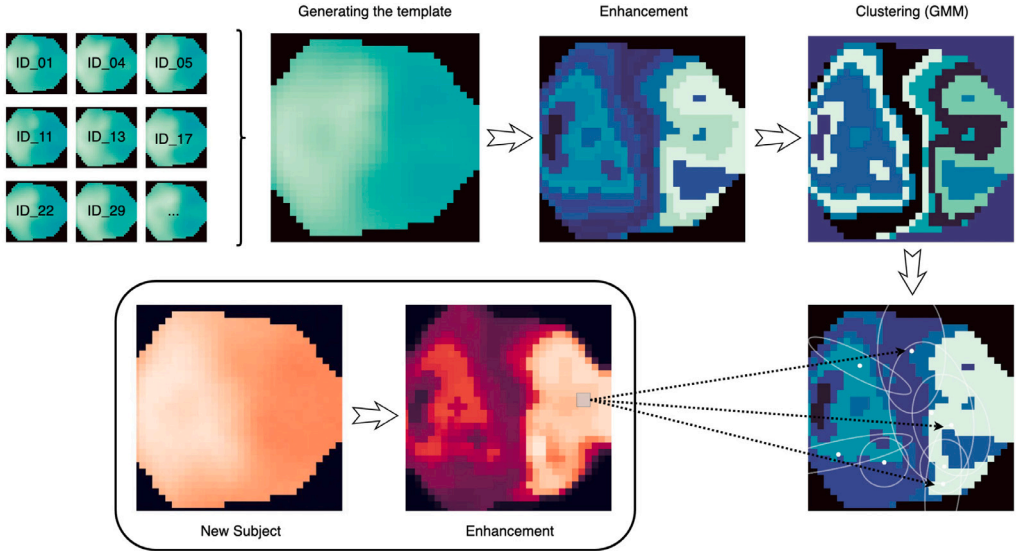

Fig. 6. General schema of the proposed methodology evaluated for CFS maps. After obtaining a reference template (transformed to enhance the differences between its intensities), we determine the probabilities of each point in any new potential subject (also transformed) belong to each component of our GMM model.

in these synthetic signals, further supporting its utility in improving classification outcomes.

The histogram-based transformation was selected after extensive experimentation and comparison with other methods, demonstrating its effectiveness in enhancing the distinctions necessary for classification of CFS maps. Alternative methods, such as Adaptive Histogram Equalization [38], Contrast-Stretching [39], and Gradient-Based Enhancement [40], are well-established; however, our approach offers the specific advantage of being tailored to the characteristics of CFS maps and EEG data. By emphasizing intensity differences through histogram transformation, we effectively address the challenge of discerning between controls and dyslexics, ultimately improving the performance of classification algorithms.

2.4. Quantization of intensity levels with GMM

GMM provides a probabilistic model that represents a mixture of multiple Gaussian distributions. In the context of image pixel clustering, GMM assumes that pixel intensities in an image are generated from a combination of different Gaussian distributions, each corresponding to a distinct cluster or region in the image [41–43]. In our context, this allows for the identification of subtle variations in phase-phase coupling patterns that might be indicative for enhanced discernment of intricate patterns in the EEG data. Moreover, the GMM approach offers several advantages: it can help to reduce the dimensionality of the input data, which makes the subsequent classification task computationally more efficient and less prone to overfitting; the GMM-based quantization can help smooth out noisy or fine-grained details in the activation maps; and it can serve as a compressed representation of the input activation maps, capturing essential features while discarding less relevant details.

The probability density function (pdf) of a GMM is expressed as a weighted sum of K Gaussian distributions:

$$p(I) = \sum_{k=1}^{K} w_k \cdot \mathcal{N}(I; \mu_k, \sigma_k^2) \tag{4}$$

where I represents the pixel CFS intensity map; w_k is the weight of the kth cluster, indicating the likelihood of a pixel belonging to that cluster[4]; and $\mathcal{N}(I; \mu_k, \sigma_k^2)$ is the Gaussian distribution with mean (center of the cluster) μ_k and variance σ_k^2 (shape and orientation of the cluster). For this work, K is assumed to be known. Nevertheless, if we want to estimate its value, we can rely on methods such as the Bayesian Information Criterion (BIC) [44], or the Akaike Information Criterion (AIC) [45].

Parameters of the GMM are estimated by means of the Expectation-Maximization (EM) algorithm [46]. After a random initialization of the parameters, this algorithm iteratively refines the parameter estimation in two steps:

- **Expectation**: For each pixel in the image, we calculate the probability the pixel belongs to each cluster using the Bayes' rule in (5), where I_n represents the intensity of the nth pixel, and $\gamma(z_{n,k})$ is the responsibility of the kth cluster for the nth pixel.

$$\gamma(z_{n,k}) = \frac{w_k \cdot \mathcal{N}(I_n; \mu_k, \sigma_k^2)}{\sum_{j=1}^{K} w_j \cdot \mathcal{N}(I_n; \mu_j, \sigma_j^2)} \tag{5}$$

- **Maximization**: Update the parameters based on the responsibilities calculated in the expectation step:

$$\begin{aligned} \mu_k^{new} &= \frac{\sum_{n=1}^{N} \gamma(z_{n,k}) \cdot I_n}{\sum_{n=1}^{N} \gamma(z_{n,k})} \\ \sigma_k^{2new} &= \frac{\sum_{n=1}^{N} \gamma(z_{n,k}) \cdot (I_n - \mu_k^{new})^2}{\sum_{n=1}^{N} \gamma(z_{n,k})} \\ w_k^{new} &= \frac{1}{N} \sum_{n=1}^{N} \gamma(z_{n,k}) \end{aligned} \tag{6}$$

Both steps are repeated iteratively until convergence. Then, each pixel is assigned to the cluster with the highest probability, leading to a segmentation of the image into distinct regions based on pixel intensities.

2.5. Intensity levels predicted by the GMM model

As shown in Fig. 6, when we average all the time segments of the controls, we generate a map (template) that serves to estimate the components of the GMM model after the quantization procedure explained before in Section 2.4.

During the evaluation of new samples (unknown a priori), we determine what is the probability that each pixel of the CFS map belongs to each component of the GMM model. Then, we assign to

[4] w_k terms must sum to 1 to ensure that the mixture represents a valid probability distribution.

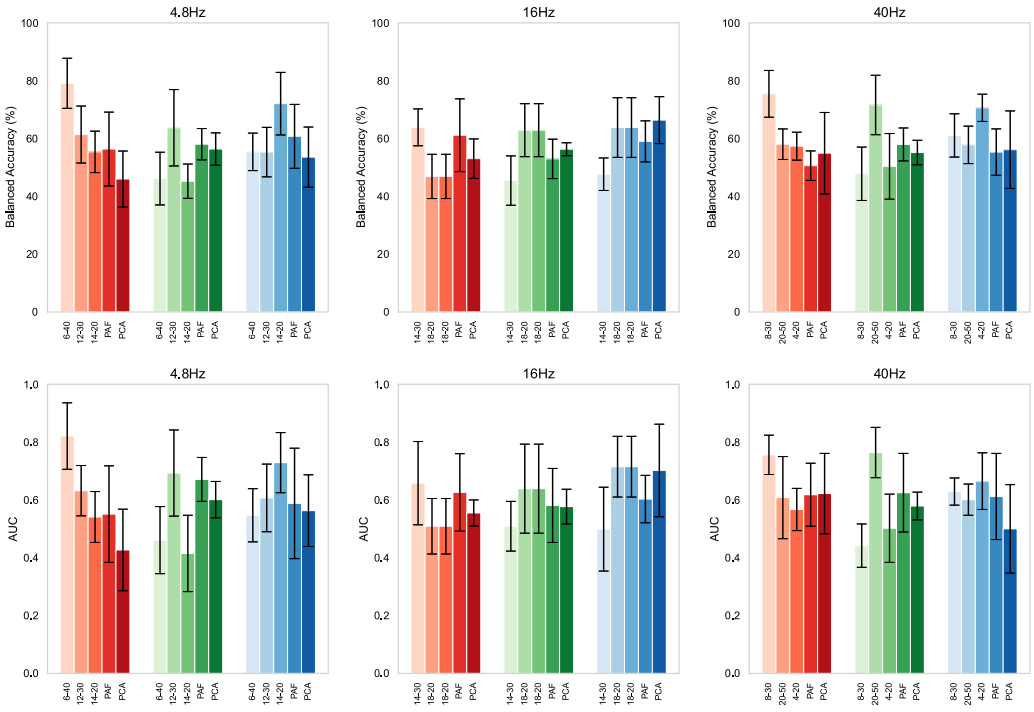

Fig. 7. Summary of classification results using our proposal (with K components and n_{Bins} bins for the histogram representation), the standard Pixels-As-Features (PAF) method and the combination of PAF+PCA approaches. Red, Green and Blue bars refer to Theta-Gamma, Alpha-Beta and Beta-Gamma band couplings respectively.

each pixel the label of the component with the highest probability. Since this membership takes into account the spatial distribution of points located in the vicinity of each component, we can hypothesize that controls will present an intensity distribution pattern similar to our reference template. Consequently, by simply counting the number of pixels assigned to each component, we will not only get a new set of transformed features physically interpretable to discern between controls and dyslexics, but also performing a dimensionality reduction method to avoid potential overfitting.

Note that using this approach we also take into account the spatial position of each pixel in the space since intensity values surrounding a centroid are more likely to belong to that component.

2.6. Classification & explainability

After the evaluation of the N_S samples in LEEDUCA platform dataset, we will get a $(N_S \times K)$ array that contains the number of points that have been labeled as belonging to the $k = 1, 2, \ldots, K$-th component of our reference template.

To systematically assess various combinations of brain coupling during auditory stimuli presentation (4.8 Hz, 16 Hz, 40 Hz) and frequency bands (Theta-Gamma, Alpha-Beta, Beta-Gamma), we constructed distinct classification pipelines. A comprehensive grid search was conducted, exploring different numbers of Gaussian Mixture Model (GMM) components and bins. The range considered was $4 - 20$ for GMM components and $20 - 100$ for histogram bins. Each pipeline involves stratifying the data and performing a 5-fold split, resulting in distinct train and test sets. As the classification method, we opted for an efficient parallel tree boosting algorithm implemented in the *XGBoost* library [47]. In each fold, the classifier undergoes evaluation using the test set, and metrics such as the Area Under the Curve (AUC) for the Receiver Operating Characteristic (ROC) curves and the balanced accuracy are computed [48,49].

Finally, to confirm the statistical significance of our findings and state that they did not occur randomly, we have conducted a rigorous assessment using permutation tests. Specifically, we employed a shuffling routine, where the labels of the training subset were shuffled, and the algorithm was re-trained using these shuffled label-data pairs. This process was repeated N_{perm} times to create a distribution of AUC values for comparison. The significance score, denoted as s in (7), quantified the likelihood of the observed AUC result (A) by comparing the model's performance accuracy with accurate labels against outcomes from the reshuffling method.[5] A lower score indicated a higher level of significance, reinforcing the robustness of our model in capturing meaningful patterns among the permutations of label assignments.

$$s = \frac{\sum_{i=1}^{N_{\text{perm}}} I(|A_i| \geq |A|)}{N_{\text{perm}}} \tag{7}$$

3. Results

For this work, we analyzed data from the 15 dyslexic individuals and 33 controls from the LEEDUCA platform dataset following the inclusion criteria described above in Section 2.1. Each of these children was given a 5-minute EEG acquisition test for each auditory stimulus (4.8 Hz, 16 Hz, 40 Hz) in ascending and descending order.

Although their EEG acquisitions could have been used directly to determine the CFS maps, we have divided them into 5-second windows to estimate up to 30 CFS values for each EEG frequency band and channel, providing a nuanced understanding of the temporal evolution of phase synchronization.

First, for each input white noise stimulus, we estimated the average maps of the CFS maps from controls in Theta-Gamma, Alpha-Beta and Beta-Gamma coupling bands. Then, within the 5-fold cross-validation loop, we transformed resulting activation maps for $nBins \in [20, 100]$ bins, and estimated the GMM with $K \in [4, 20]$ components. Thus, each time a test sample was evaluated, we determined the probability of

[5] A_i is the AUC value for the ith permutation, then $I(|A_i| \geq |A|)$ is the indicator function that evaluates whether the AUC value for the ith permutation is greater than or equal to the ground AUC value obtained with the correct labels.

Table 1
Balanced Accuracy (bAcc) and Area Under the Curve (AUC) results for the [4.8 Hz, 16 Hz, 40 Hz] stimuli using XGBoost classifiers. Comparison between our proposal (using K components for the GMM and histograms with $nBins$ bins), the standard Pixels-As-Features approach (classifying all the input features which might be leading to overfitted results) and transforming the CFS activations trough Principal Component Analysis (90% of explained variability) before their classification. Note that there are two rows repeated for the 16 Hz stimulus since parameters that best fitted the AUC for the Alpha-Beta and Beta-Gamma couplings were found to be the same.

Stimulus	K	nBins	Theta-Gamma		Alpha-Beta		Beta-Gamma	
			bAcc	AUC	bAcc	AUC	bAcc	AUC
4.8 Hz	6	40	**79.09%±8.66%**	**0.821 ± 0.115**	46.14%±9.12%	0.461 ± 0.116	55.38%±6.48%	0.547 ± 0.092
	12	30	61.37%±9.85%	0.632 ± 0.087	**63.71%±13.21%**	**0.693 ± 0.149**	55.30%±8.56%	0.607 ± 0.117
	14	20	55.38%±7.17%	0.541 ± 0.088	45.23%±5.93%	0.415 ± 0.132	**72.05%±10.82%**	**0.729 ± 0.104**
	PAF		56.36%±12.77%	0.551 ± 0.167	58.03%±5.41%	0.671 ± 0.076	60.75%±11.05%	0.588 ± 0.191
	PAF+PCA		45.98%±9.69%	0.427 ± 0.141	56.36%±5.59%	0.601 ± 0.063	53.56%±10.41%	0.563 ± 0.124
16 Hz	14	30	**63.86%±6.38%**	**0.658 ± 0.144**	45.45%±8.54%	0.509 ± 0.086	47.65%±5.62%	0.499 ± 0.145
	18	20	46.89%±7.65%	0.509 ± 0.096	**62.88%±9.16%**	**0.639 ± 0.154**	**63.79%±10.32%**	**0.715 ± 0.105**
	18	20	46.89%±7.65%	0.509 ± 0.096	**62.88%±9.16%**	**0.639 ± 0.154**	**63.79%±10.32%**	**0.715 ± 0.105**
	PAF		61.13%±12.58%	0.626 ± 0.134	52.95%±6.82%	0.581 ± 0.128	59.01%±7.10%	0.603 ± 0.082
	PAF+PCA		53.03%±6.83%	0.555 ± 0.045	56.28%±2.24%	0.577 ± 0.060	66.36%±8.11%	0.702 ± 0.160
40 Hz	8	30	**75.45%±8.09%**	**0.756 ± 0.068**	47.80%±9.23%	0.442 ± 0.075	61.06%±7.48%	0.629 ± 0.047
	20	50	58.03%±5.28%	0.608 ± 0.142	**71.59%±10.28%**	**0.764 ± 0.087**	57.80%±6.48%	0.601 ± 0.054
	4	20	57.35%±4.83%	0.567 ± 0.073	50.37%±11.35%	0.502 ± 0.118	**70.61%±4.71%**	**0.665 ± 0.098**
	PAF		50.60%±5.11%	0.618 ± 0.109	57.95%±5.69%	0.625 ± 0.136	55.30%±8.03%	0.612 ± 0.149
	PAF+PCA		54.92%±14.09%	0.622 ± 0.139	55.15%±4.24%	0.579 ± 0.048	56.13%±13.41%	0.500 ± 0.153

each pixel is assigned to the kth component and used this feature vector as input for the classifier.

Table 1, and its summary in Fig. 7, presents the classification results for the different auditory stimuli presentations (4.8 Hz, 16 Hz, 40 Hz) and frequency coupling bands (Theta-Gamma, Alpha-Beta, and Beta-Gamma) regarding the n_{Bins} and K parameters for the grid search. Additionally, we have also compared our results with both the standard PAF approach and the transformed versions of the CFS maps through Principal Component Analysis (PCA), across these different stimuli frequencies.

In interpreting these results, it is crucial to recognize the inherent complexity of the classification task and the variability introduced by different parameter settings. While some results may hover around 50%, this reflects the challenging nature of identifying subtle dyslexia-related neural patterns and the necessity of determining suitable K and n_{Bins} parameters for each scenario. Our method is specifically designed for scenarios involving images with few differences, making classification tasks inherently difficult. We have compared our approach with the PAF and PAF combined with PCA approaches. These comparisons demonstrate that both PAF and PAF+PCA also exhibit similar performance issues, underscoring the difficulty of the task. Notably, our method shows substantial improvements in the Theta-Gamma and Beta-Gamma couplings at the 4.8 Hz auditory stimulus and across all couplings at the 40 Hz auditory stimulus when suitable parameters are determined. These findings highlight the importance of specific parameter configurations and stimuli frequencies, as well as the efficacy of our method in enhancing classification performance.

In addition to this, we have included in Fig. 8 the permutation tests results associated to the classification experiments in Table 1.

4. Discussion

In recent years, research in neuroscience has increasingly turned towards understanding the intricate dynamics of brain function, especially concerning healthy and pathological conditions [50,51]. In this context, Cross-Frequency Coupling (CFC) has emerged as a valuable tool for unraveling the complexities of neural communication [26,52,53]. CFC analysis provides a unique perspective into dynamic interactions among different neural rhythms. This offers us valuable insights into how various brain regions interact during cognitive tasks, like reading.

As we try to make sense of these complex neural processes, the application of sophisticated analytical techniques becomes imperative, particularly in domains where the complexity of conditions is pronounced. In the specific context of reading disabilities, the challenge lies not only in elucidating the intricate neural underpinnings but also in addressing the inherent heterogeneity within the affected population [4,5], and the potential links to some genetic mutations [54]. Therefore, as we delve deeper into the complexities of dyslexia, sophisticated analytical techniques become crucial for making sense of the multifaceted data derived from neuroimaging.

The results in Table 1 arise from an experiment that utilized low-level auditory processing of non-speech stimuli related to Spanish speech units, such as syllables (4.8 Hz), intrasyllabic segmentation rhythms (16 Hz), and phonemes (40 Hz) in skilled and dyslexic seven-year-old readers. According to the temporal sampling framework [55], auditory processing is expected to be disrupted in dyslexia, specifically with an emphasis on syllabic processing. Additionally, Giraud and Poepple [6] link the phonological deficit found in dyslexia to the processing of phonemes in higher frequencies, such as gamma oscillations.

In Table 1, the features obtained from CFS between frequency bands Beta-Gamma and Theta-Gamma achieve the best results for all stimuli. The Beta-Gamma coupling closely aligns with the rate at which the brain processes phonemes following the segmentation of input speech. During this process, synchronous bursts of neural activity occur in low-gamma ranges (20-40 Hz) in auditory cortices [56]. Therefore, anomalies in the generation of gamma oscillations could have significant consequences for phonological processing. On the other hand, Theta-Gamma coupling plays a crucial role in cognitive control and working memory, facilitating the integration of information across different neural assemblies. This integration is essential for tasks such as speech processing and reading, which are impaired in dyslexic individuals. Our results highlight the sensitivity of our proposed method to the altered mechanisms in neural oscillations associated with the phonological deficit, particularly those related to phonemic representations and the cognitive control required for reading.

The application of our GMM-based method results not only in similar classification rates than those obtained by directly classifying activations of CFS maps in the original space (PAF, in Table 1) but also with a clear advantage: while the PAF approach requires to classify $32 \times 32 = 1024$ input features, thanks to the enhancement of the differences between intensity values in original CFS maps and the GMM-based clustering approach, we manage to reduce the input space dimensionality to less than 20 features in the worst-case scenario. This helps us to prevent potential overfitting and provides us a compressed representation of EEG activation maps.

The validation of our results is robustly established through permutation testing. This involves shuffling the labels and repeatedly retraining the classifier to ensure that our findings are not simply due

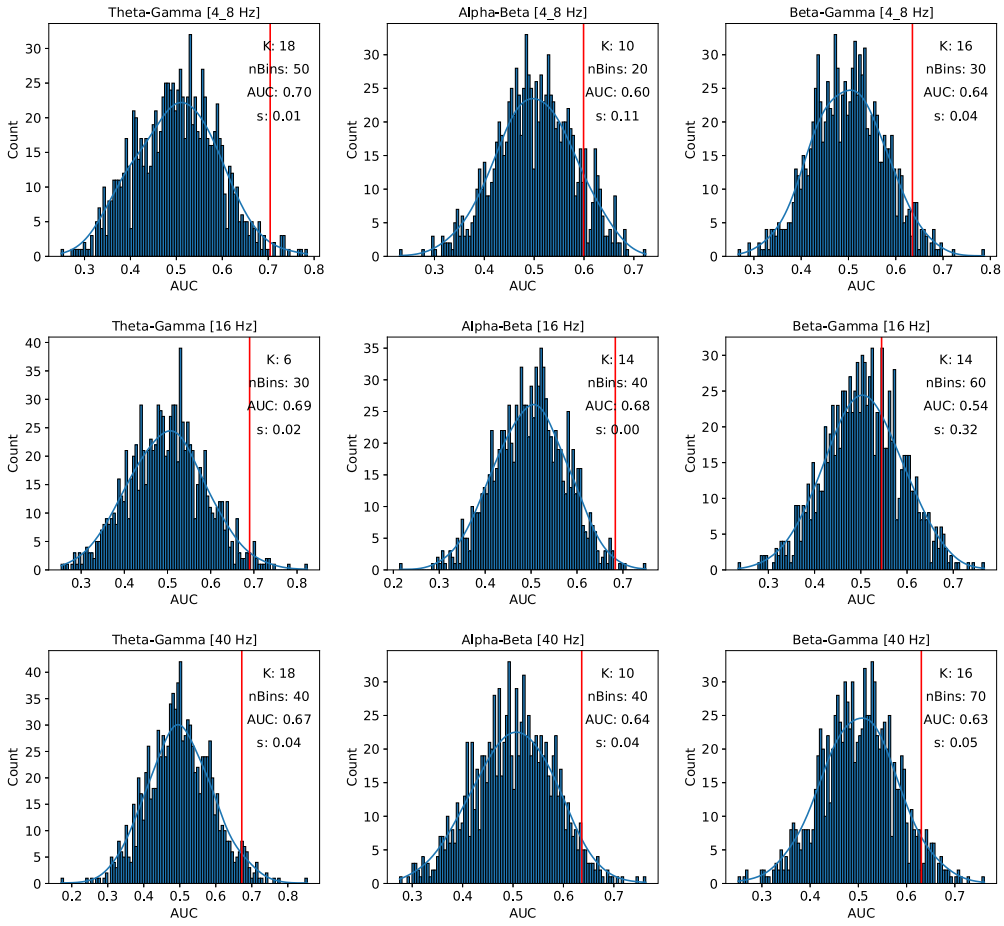

Fig. 8. Permutations results for [4.8 Hz, 16 Hz and 40 Hz] stimulus. In red, it is shown the truth AUC value obtained.

to random chance. Fig. 8 illustrates the results of these permutation tests for the optimally selected combinations of channels, components, and bins. The histogram represents the distribution of the AUC scores achieved from each permutation, with the red line indicating the actual AUC value (the score derived without label permutation). In the figure, we can see that significance levels (score s) below 0.05 are achieved in all bands except for the Beta-Gamma coupling at the 16 Hz auditory stimulus. This significance level guarantees that the AUC is not obtained by chance, thus validating the results obtained. The number of components for these results ranges between 4 and 18, and the bins range between 20 and 50.

While the results of this study are very promising, the dimensional reduction arising from pixel counting within each component of the reference template makes it challenging to spatially identify compensation mechanisms, as described in [57,58]. Thus, and in addition to the limited size of the dataset, we propose the adaptation of the current approach to address this limitation.

5. Conclusions

This study presents a novel and promising approach for exploring differential patterns of dyslexia in neural oscillations using CFC analysis of EEG signals. First, we have investigated the neural mechanisms contained in intraelectrode brain rhythms arising from an EEG experiment with non-interactive auditory stimuli presented to skilled and dyslexic seven-year-old readers. This information has been obtained on the basis of a CFS exploratory analysis and transformed into images sequences. Achieving a representation that preserves the temporal evolution of the phase synchronization with spatial EEG channel location information.

Secondly, we have improved the extraction of information from these image sequences by employing a temporal averaging approach and by enhancing differences in the CFS intensity maps with a transformation of each pixel that accentuate the edges of the regions we want to cluster. This allows the application of probabilistic models for the pixel-wise clustering of the transformed CFS maps. We have employed GMM to identify subtle variations in phase-phase coupling patterns with potential discriminative information.

Finally, this approach using GMM attain a dimensional reduction of the input data, which improve computational efficiency and reduce the risk of overfitting. Thus, allowing us to differentiate between controls and DD subjects reaching an AUC of up to 82.1% for the Theta-Gamma CFS. Furthermore, it accomplish a compressed representation of CFS activation maps, capturing essential features while discarding less relevant details. All this supports the potential of harnessing advanced analytical techniques, combining neuroscience and AI, to unravel the multifaceted nature of dyslexia.

CRediT authorship contribution statement

Diego Castillo-Barnes: Writing – review & editing, Writing – original draft, Visualization, Validation, Software, Methodology, Investigation, Formal analysis, Conceptualization. **Nicolás J. Gallego-Molina:** Methodology, Formal analysis, Data curation, Conceptualization. **Marco A. Formoso:** Validation, Software, Resources. **Andrés Ortiz:** Supervision, Resources, Project administration, Funding acquisition, Conceptualization. **Patrícia Figueiredo:** Supervision, Resources, Project administration, Funding acquisition. **Juan L. Luque:** Project administration, Funding acquisition, Conceptualization.

Acknowledgments

This research is part of the PID2022-137461NB-C32 funded by MICIU/AEI/10.13039/501100011033 and by ERDF/EU. Work by D.C.-B. is part of the grant FJC2021-048082-I funded by MICIU/AEI/10.13039/501100011033 and by European Union NextGenerationEU/PRTR. M.-A.F. grant PRE2019087350 funded by MICIU/AEI/10.13039/501100011033 by "ESF Investing in your future". LARSyS funding (DOI: 10.54499/LA/P/0083/2020, 10.54499/UIDP/50009/2020, and the 10.54499/UIDB/50009/2020). Funding for open access charge: Universidad de Málaga/CBUA.

Declaration of competing interest

The authors declare that they have no known competing financial interests or personal relationships that could have appeared to influence the work reported in this paper.

References

[1] Reid G. The SAGE handbook of dyslexia. SAGE Publications; 2008.
[2] Hulme C, Snowling M. Reading disorders and dyslexia. Curr Opin Pediatrics 2016;28:731–5.
[3] McArthur G, Kohnen S, Larsen L, Jones K, et al. Getting to grips with the heterogeneity of developmental dyslexia. Cogn Neuropsychol 2013;30:1–24.
[4] Pacheco A, Reis A, Araújo S, Inácio F, et al. Dyslexia heterogeneity: cognitive profiling of portuguese children with dyslexia. Read Writ 2014;27:1529–45.
[5] Zoubrinetzky R, Bielle F, Valdois S. New insights on developmental dyslexia subtypes: Heterogeneity of mixed reading profiles. PLoS One 2014;9:e99337.
[6] Giraud A, Poeppel D. Cortical oscillations and speech processing: emerging computational principles and operations. Nat Neurosci 2012;15:511–7.
[7] Soltész F, Szűcs D, Leong V, White S, Goswami U. Differential entrainment of Neuroelectric Delta oscillations in developmental dyslexia. PLoS One 2013;8:e76608.
[8] Gross J, Hoogenboom N, Thut G, Schyns P, et al. Speech rhythms and multiplexed oscillatory sensory coding in the human brain. PLoS Biol 2013;11:e1001752.
[9] Keitel A, Gross J, Kayser C. Perceptually relevant speech tracking in auditory and motor cortex reflects distinct linguistic features. PLoS Biol 2018;16:e2004473.
[10] Keshavarzi M, Mandke K, Macfarlane A, Parvez L, et al. Atypical beta-band effects in children with dyslexia in response to rhythmic audio-visual speech. Clin Neurophysiol 2024;160:47–55.
[11] Gallego-Molina N, Formoso M, Ortiz A, Martínez-Murcia F, Luque J. Temporal EigenPAC for dyslexia diagnosis. In: Advances in computational intelligence. 2021, p. 45–56.
[12] Gallego-Molina N, Ortiz A, Martínez-Murcia F, Rodríguez-Rodríguez I. Unraveling dyslexia-related connectivity patterns in EEG signals by Holo-Hilbert spectral analysis. In: Artificial intelligence in neuroscience: affective analysis and health applications. 2022, p. 43–52.
[13] Formoso M, Ortiz A, Martinez-Murcia F, Gallego N, Luque J. Detecting phase-synchrony connectivity anomalies in EEG signals. Application to dyslexia diagnosis. Sensors 2021;21:7061.
[14] Gallego-Molina N, Ortiz A, Martínez-Murcia F, Formoso M, Giménez A. Complex network modeling of EEG band coupling in dyslexia: An exploratory analysis of auditory processing and diagnosis. Knowl-Based Syst 2022;240:108098.
[15] Attaheri A, Ní Choisdealbha Á, Liberto G, Rocha S, et al. Delta- and theta-band cortical tracking and phase–amplitude coupling to sung speech by infants. NeuroImage 2022;247:118698.
[16] Nadalin J, Martinet L, Blackwood E, Lo M, et al. A statistical framework to assess cross-frequency coupling while accounting for confounding analysis effects. ELife 2019;8.
[17] Hülsemann M, Naumann E, Rasch B. Quantification of phase-amplitude coupling in neuronal oscillations: Comparison of phase-locking value, mean vector length, modulation index, and generalized-linear-modeling-cross-frequency-coupling. Front Neurosci 2019;13.
[18] Martínez-Cancino R, Heng J, Delorme A, Kreutz-Delgado K, et al. Measuring transient phase–amplitude coupling using local mutual information. NeuroImage 2019;185:361–78.
[19] Duin RPW. Classifiers in almost empty spaces. In: Proceedings 15th International Conference on Pattern Recognition. ICPR-2000. IEEE Comput. Soc; 2000, http://dx.doi.org/10.1109/icpr.2000.906006, ICPR-00.
[20] Ortiz A, Martinez-Murcia F, Luque J, Giménez A, et al. Dyslexia diagnosis by EEG temporal and spectral descriptors: An anomaly detection approach. Int J Neural Syst 2020;30:2050029.
[21] Wang G, Teng C, Li K, Zhang Z, Yan X. The removal of EOG artifacts from EEG signals using independent component analysis and multivariate empirical mode decomposition. IEEE J Biomed Health Inf 2016;20:1301–8.
[22] Biel A, Minarik T, Sauseng P. EEG cross-frequency phase synchronization as an index of memory matching in visual search. NeuroImage 2021;235:117971.
[23] Jiang X, Bian G, Tian Z. Removal of artifacts from EEG signals: A review. Sensors 2019;19:987.
[24] Li R, Yang D, Fang F, Hong K, et al. Concurrent fNIRS and EEG for brain function investigation: A systematic, methodology-focused review. Sensors 2022;22:5865.
[25] Palva J, Palva S, Kaila K. Phase synchrony among neuronal oscillations in the human cortex. J Neurosci 2005;25:3962–72.
[26] Scheffer-Teixeira R, Tort A. On cross-frequency phase-phase coupling between theta and gamma oscillations in the hippocampus. ELife 2016;5.
[27] Rosenblum M, Pikovsky A, Kurths J. Phase synchronization of chaotic oscillators. Phys Rev Lett 1996;76:1804–7.
[28] Stam C, Nolte G, Daffertshofer A. Phase lag index: Assessment of functional connectivity from multi channel EEG and MEG with diminished bias from common sources. Hum Brain Map 2007;28:1178–93.
[29] Belluscio M, Mizuseki K, Schmidt R, Kempter R, Buzsáki G. Cross-frequency phase–phase coupling between theta and Gamma oscillations in the hippocampus. J Neurosci 2012;32:423–35.
[30] Dvorak D, Fenton A. Toward a proper estimation of phase–amplitude coupling in neural oscillations. J Neurosci Methods 2014;225:42–56.
[31] Liu C, Chen W, Zhang T. Wavelet-Hilbert transform based bidirectional least squares grey transform and modified binary grey wolf optimization for the identification of epileptic EEGs. Biocybern Biomed Eng 2023;43:442–62.
[32] Bashivan P, Rish I, Yeasin M, Codella N. Learning representations from EEG with deep recurrent-convolutional neural networks. 2015.
[33] Alfeld P. A trivariate clough—tocher scheme for tetrahedral data. Comput Aided Geom Design 1984;1:169–81.
[34] Kimppa L, Shtyrov Y, Partanen E, Kujala T. Impaired neural mechanism for online novel word acquisition in dyslexic children. Sci Rep 2018;8.
[35] Thiede A, Glerean E, Kujala T, Parkkonen L. Atypical MEG inter-subject correlation during listening to continuous natural speech in dyslexia. NeuroImage 2020;216:116799.
[36] Attaheri A, Choisdealbha A, Rocha S, Brusini P, et al. Infant low-frequency EEG cortical power, cortical tracking and phase–amplitude coupling predicts language a year later. Cold Spring Harbor Laboratory; 2022.
[37] Majkowski A, Oskwarek Ł, Kołodziej M, Rak R. An attempt to localize brain electrical activity sources using EEG with limited number of electrodes. Biocybern Biomed Eng 2016;36:686–96.
[38] Pizer S, Amburn E, Austin J, Cromartie R, et al. Adaptive histogram equalization and its variations. Comput Vis Graph Image Process 1987;39:355–68.
[39] Yang C. Image enhancement by modified contrast-stretching manipulation. Opt Laser Technol 2006;38:196–201.
[40] Chaple G, Daruwala R, Gofane M. Comparisions of Robert, Prewitt, Sobel operator based edge detection methods for real time uses on FPGA. In: 2015 international conference on technologies for sustainable development. 2015.
[41] Li R, Perneczky R, Yakushev I, Förster S, et al. Gaussian mixture models and model selection for [18F] fluorodeoxyglucose positron emission tomography classification in Alzheimer's disease. PLoS One 2015;10:e0122731.
[42] Derntl A, Plant C. Clustering techniques for neuroimaging applications. WIREs Data Min Knowl Discov 2015;6:22–36.
[43] Churchill N, Madsen K, Mørup M. The functional segregation and integration model: Mixture model representations of consistent and variable group-level connectivity in fMRI. Neural Comput 2016;28:2250–90.
[44] Schwarz G, et al. Estimating the dimension of a model. Ann Statist 1978;6:461–4.
[45] Akaike H. A new look at the statistical model identification. IEEE Trans Autom Control 1974;19:716–23.
[46] Castillo-Barnes D, Martinez-Murcia F, Ramírez J, Górriz J, Salas-Gonzalez D. Expectation-maximization algorithm for finite mixture of α-stable distributions. Neurocomputing 2020;413:210–6.
[47] Chen T, Guestrin C. XGBoost: A scalable tree boosting system. In: Proceedings of the 22nd ACM SIGKDD international conference on knowledge discovery and data mining. 2016.
[48] Faraggi D, Reiser B. Estimation of the area under the ROC curve. Stat Med 2002;21:3093–106.
[49] Brodersen K, Ong C, Stephan K, Buhmann J. The balanced accuracy and its posterior distribution. In: 2010 20th international conference on pattern recognition. 2010.
[50] Fujii M, Maesawa S, Ishiai S, Iwami K, et al. Neural basis of language: An overview of an evolving model. Neurol Medico-Chirurgica 2016;56:379–86.
[51] Górriz J, Illán I, Marquina A, Arco J, et al. Computational approaches to explainable artificial intelligence: Advances in theory, applications and trends. Inform Fus 2023;101945.
[52] Canolty R, Knight R. The functional role of cross-frequency coupling. Trends in Cognitive Sciences 2010;14:506–15.
[53] Aru J, Aru J, Priesemann V, Wibral M, et al. Untangling cross-frequency coupling in neuroscience. Curr Opin Neurobiol 2015;31:51–61.

[54] Gialluisi A, Andlauer T, Mirza-Schreiber N, Moll K, et al. Genome-wide association study reveals new insights into the heritability and genetic correlates of developmental dyslexia. Mol Psychiatry 2020;26:3004–17.
[55] Goswami U. A temporal sampling framework for developmental dyslexia. Trends in Cognitive Sciences 2011;15:3–10.
[56] Giraud A, Ramus F. Neurogenetics and auditory processing in developmental dyslexia. Curr Opin Neurobiol 2013;23:37–42.
[57] Arns M, Peters S, Breteler R, Verhoeven L. Different brain activation patterns in dyslexic children: Evidence from EEG power and coherence patterns for the double-deficit theory of dyslexia. J Integr Neurosci 2007;6:175–90.
[58] Di Liberto G, Peter V, Kalashnikova M, Goswami U, et al. Atypical cortical entrainment to speech in the right hemisphere underpins phonemic deficits in dyslexia. NeuroImage 2018;175:70–9.